Journal of Electronic Materials (2022) 51:1900–1904
https://doi.org/10.1007/s11664-022-09454-5

TOPICAL COLLECTION: SYNTHESIS AND ADVANCED CHARACTERIZATION OF MAGNETIC OXIDES

Structural, Surface, and Electronic Structure Properties of Ag^- Ion-Implanted $SrVO_3$ Thin Films

Aditya Sharma[1] · **Ksh. Devarani Devi**[1,2] · **Mayora Varshney**[3] · **Himani Saraswat**[1] · **Surekha Chaudhary**[1] · **Byeong-hyeon Lee**[4] · **So-Hee Kim**[4] · **Sung Ok Won**[4] · **Keun Hwa Chae**[4] · **Ankush Vij**[5] · **Ram K. Sharma**[6] · **Hyun-Joon Shin**[7]

Received: 26 October 2021 / Accepted: 13 January 2022 / Published online: 16 February 2022
© The Minerals, Metals & Materials Society 2022

Abstract

$SrVO_3$ films have been deposited on quartz substrates using radiofrequency (RF) sputtering technique. Ag^- ions have been implanted with three fluences: 1×10^{15} ions/cm^2, 3×10^{15} ions/cm^2, and 5×10^{15} ions/cm^2. The glancing-angle x-ray diffraction (GIXRD) results exhibited a decrease in the peak intensity; however, the results ruled out the possibility of other secondary phase formation upon increasing the Ag^- ion fluence. Field emission scanning electron microscopy (FESEM) results revealed that Ag implantation has sputtered the surface layer and created rough/emptied films. Significant broadening/splitting of V L_2 near-edge x-ray absorption fine structure (NEXAFS) spectra convey the incorporation of Ag 4*d* states in the energy band structure of $SrVO_3$ and electronic transitions from V $2p_{1/2}$ states to the Ag-related states. O K-edge spectra have ruled out the charge transfer of O 1*s* orbits to the Ag states, even upon increasing the Ag concentration, and nullified the formation of AgO types of secondary phases.

Keywords $SrVO_3$ · implantation · defects · NEXAFS

✉ Aditya Sharma
adityaiuac@gmail.com

✉ Hyun-Joon Shin
shin@chungbuk.ac.kr

[1] Department of Physics, Manav Rachna University, Faridabad, Haryana 124001, India

[2] Inter University Accelerator Centre, Aruna Asaf Ali Marg, New Delhi 110067, India

[3] Department of Applied Physics, School of Vocational and Applied Sciences, Gautam Buddha University, Greater Noida, Uttar Pradesh 201312, India

[4] Advance Analysis Centre, Korea Institute of Science and Technology (KIST), 02792 Seoul, South Korea

[5] Department of Physics, University of Petroleum and Energy Studies, Dehradun, Uttarakhand 248007, India

[6] Centre for Interdisciplinary Research and Innovation, University of Petroleum and Energy Studies, Dehradun 248007, India

[7] Department of Physics, Chungbuk National University, Cheongju 28644, South Korea

Introduction

ABO_3 perovskite-type $SrVO_3$ compound has been studied for its intriguing structural and electronic structure assets[1–4] and various applications in perovskite solar cells, high-temperature solid oxide fuel cells, high-density dynamic random-access memory, etc.[5–8] The cubic structured $SrVO_3$ obeys $3d^1$ electronic configuration which provides an admixture of V 3*d* orbitals with O 2*p* orbitals. The non-bonding O 2*p* orbitals form the top of the valence band and the anti-bonding O 2*p* and V 3*d* orbitals constitute the bottom of the conduction band.[1,2] It has been observed that polymorphous phases possess distortion in the V–O polyhedrons and provide diverse electronic properties to the compound.[3,4] The native defects in $SrVO_3$ and $LaVO_3$ have evoked the origin of intriguing magnetic properties in the $LaVO_3$/$SrVO_3$ superlattice.[9–11] Likewise, the electronic structure, charge carrier concentration/mobility, bandgap energy, and conductivity can be engineered by doping of the foreign elements at either V or Sr sites.[12,13] However, the properties and, hence, applications of doped ABO_3-type perovskites largely rely on the doping methods.[14,15]

In the context of foreign element doping, the ion implantation technique has several advantages like a high-purity process under high vacuum, depth control, concentration control, doping area control, etc.[16–20] The factors that influence the properties of implanted materials are ion energy, ion fluence, and the nature of implanted ions. In this process, the implanted ions not only occupy the substitutional sites of host atoms but also create a large amount of point/cluster defects. Thus, control of these factors paves a way to manipulate the properties of materials systematically. There are only a few studies available for ion implantation-induced modification in $SrVO_3$.[21,22] Cu ion implantation in $SrVO_3$ could facilitate lattice parameter changes and reduction in the bandgap energy via accumulating the Cu defect states.[22] Analogous to the Cu atoms, the Ag atoms may facilitate the defect states of the $SrVO_3$ compound. The partly occupied 4*d* orbitals of Ag (i.e., $4d^9$) are much more dispersive than that of 3*d* orbitals of Cu. Additionally, the Ag atoms are larger than the Cu atoms. Therefore, with Ag doping in $SrVO_3$, one may expect larger V–O distortion and extended overlapping of Ag (4*d*) wavefunctions with the V (3*d*) wavefunctions when compared to the case of Cu doping in $SrVO_3$. In this study, 90 keV Ag^- ions were implanted in $SrVO_3$ thin films. Three ion fluences were employed to investigate the extrinsic defect concentration dependency on the structural, surface morphology, and electronic structure assets of $SrVO_3$ thin films.

Experimental Details

$SrVO_3$ thin films were grown on quartz substrates by radiofrequency (RF) sputtering technique under the same experimental conditions as described elsewhere[4] with the sputtering time of 60 min. The Ag^- ions, with 90 keV of energy, were implanted in the prepared films with three different fluences of 1×10^{15} ions/cm^2, 3×10^{15} ions/cm^2, and 5×10^{15} ions/cm^2 using a source of negative ions by cesium sputtering (SNICS) at IUAC, New Delhi, India. The vacuum of the implantation chamber was 5×10^{-7} torr. As-deposited and ion-implanted films were post-annealed at 600^0C in air for 4 hrs. The glancing-angle x-ray diffraction (GIXRD) measurements were performed using the Rigaku D/Max 2500 x-ray diffractometer (Cu Kα radiation; $\lambda = 1.5418$ Å) with an incidence angle of 1^0 and a scan speed of 2^0 min^{-1}. The lattice parameters and (hkl) values were evaluated using the JADE software package. Field emission scanning electron microscopy (FESEM) measurements were performed using a Hitachi (Regulus 8230) machine. Near-edge x-ray absorption fine structure (NEXAFS) measurements were collected, in total electron yield (TEY), at the V L edge and O K-edge, at the 10D XAS-KIST soft x-ray beamline at the Pohang Accelerator Laboratory (PAL), South Korea. In a typical NEXAFS measurement, the incident photon flux (*I*o) is measured by Au mesh placed in the path of the beam. Samples are mounted on a Cu holder with the help of carbon tape and placed in a high vacuum (5×10^{-8} torr). In the TEY method of data collection, all of the electrons (i.e., photoelectrons and Auger electrons) are collected with a Channeltron electron multiplier. In this mode of data collection, the low-energy electrons (<20 eV, with a large mean free path) are collected. TEY method is very effective for the topmost surface layers (i.e., for thin films). The energy resolution of the used beamline was better than 0.6 eV (at the O K-edge).

Results and Discussion

Stopping and range of ions in matter (SRIM; www.srim.org) calculations were performed to discern the cross over the ion range, straggling, electronic energy loss (S_e) and nuclear energy loss (S_n) of Ag^- ions in $SrVO_3$ lattice. The range of Ag^- ions in $SrVO_3$ is 276 Å. The longitudinal and transversal straggling are 106 Å and 73 Å, respectively, as shown in supplementary Figure S1. It is clear from Figure S1 that S_n is greater than S_e, and thus, various defects are expected to be formed due to S_n governing effects, such as point/cluster defect formation and surface sputtering. Supplementary Figure S2 shows the GIXRD data of as-deposited and as-implanted (ion fluence: 1×10^{15} ions/cm^2, 3×10^{15} ions/cm^2, and 5×10^{15} ions/cm^2) $SrVO_3$ thin films. It is noticeable that such a set of films do not show any intense diffraction peaks and reflect their poor crystalline or amorphous nature. The amorphous nature of as-deposited films may be due to the non-stoichiometric adsorption of constituent elements (Sr, V, and O) onto the quartz substrates. Moreover, the low-energy (90 keV) Ag^- ions may have not supplied enough energy to grow the crystalline phases of $SrVO_3$ compound. Therefore, the as-implanted samples are also amorphous.

Figure 1 shows the GIXRD patterns of pure and Ag^- ion-implanted $SrVO_3$ films annealed at 600°C. It is noticeable that several intense diffraction peaks are present in all of the samples and are strengthening the formation of polycrystalline films after the annealing with orthorhombic $SrVO_3$ phase ($a = 6.156$ (12) Å, $b = 7.701(15)$ Å, $c = 5.367(07)$ Å, $\alpha = \beta = \gamma = 90°$; the numbers in parentheses represent errors in the lattice parameters). The bottom panel of Fig. 1 shows the XRD profile from JCPDS file #06-9548. It is noticeable that major diffraction patterns of pure and Ag ion-implanted $SrVO_3$ films closely match with the XRD patterns of the given JCPDS file and confirm the orthorhombic phase in the $SrVO_3$ thin films. It is noticeable that the XRD peak intensity of the major peak [i.e., (200)] is diminished and that other low-intensity peaks [for example, (111)] are nearly vanished upon increasing the ion fluence of Ag ions. It could be due to the ion implantation-induced damage of $SrVO_3$

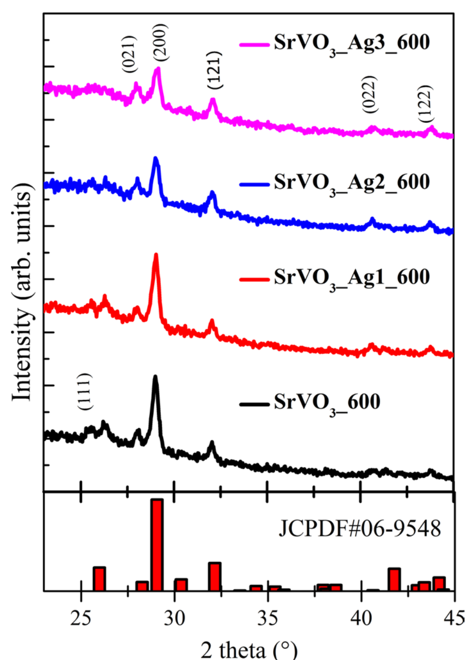

Fig. 1 GIXRD patterns of samples annealed at 600°C: pure $SrVO_3$ ($SrVO_3$_600), 1 × 10^{15} ions/cm^2 implanted $SrVO_3$ films ($SrVO_3$_Ag1_600), 3 × 10^{15} ions/cm^2 implanted $SrVO_3$ films ($SrVO_3$_Ag2_600), and 5 × 10^{15} ions/cm^2 implanted $SrVO_3$ films ($SrVO_3$_Ag3_600). The bottom panel shows the XRD patterns from the JCPDS file #06-9548.

lattice and various defect/stacking fault formations.[19,22] Moreover, no AgO or other V oxide phases were detected under the detection limit of the used x-ray diffractometer.

Surface morphology (2D view) was investigated using FESEM, and film thickness was estimated using the cross-sectional FESEM measurements. It is noticeable from Fig. 2a–b that pure $SrVO_3$ (annealed at 600°C) film shows a packed and granular morphology with a film thickness of ~ 135 nm. The FESEM images of Ag^- ions implanted (with ion fluence of 5 × 10^{15} ion/cm^2 and annealed at 600°C) sample is showing a rough morphology with some voids, and the film thickness is ~ 95 nm. The induced roughness and reduction in film thickness may be due to the Ag^- ion-induced surface sputtering of $SrVO_3$ thin film and is analogous to the previous reports.[19,22] The EDS results of the Ag^- ion-implanted (5 × 10^{15} ion/cm^2) sample are presented in supplementary Figure S3 which conveys the even distribution of elements in the film. The atm% of elements is also provided in supplementary Table 1.

Figure 3 shows NEXAFS spectra of pure and Ag^- ion-implanted $SrVO_3$ thin films (annealed at 600°C). The spectral features between 515 eV and 528 eV are of the V L-edge and correspond to the V 2*p* to V 3*d* electronic transitions.[23–25] There are two distinct peaks in the V L-edge spectrum of pure $SrVO_3$ film, marked by L_3 and L_2. These peaks originate from V $2p_{3/2}$ and V $2p_{1/2}$ core level transitions

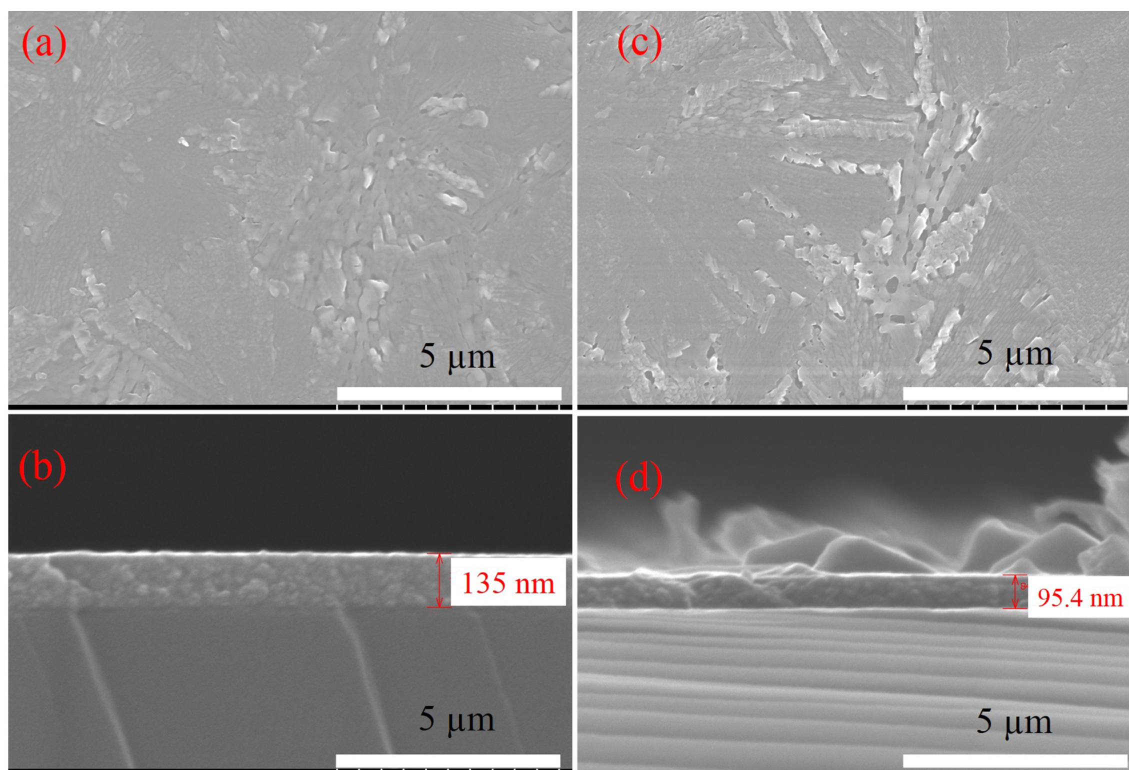

Fig. 2 FESEM images (a–b) of $SrVO_3$_600 and (c–d) of $SrVO_3$_Ag3_600 samples.

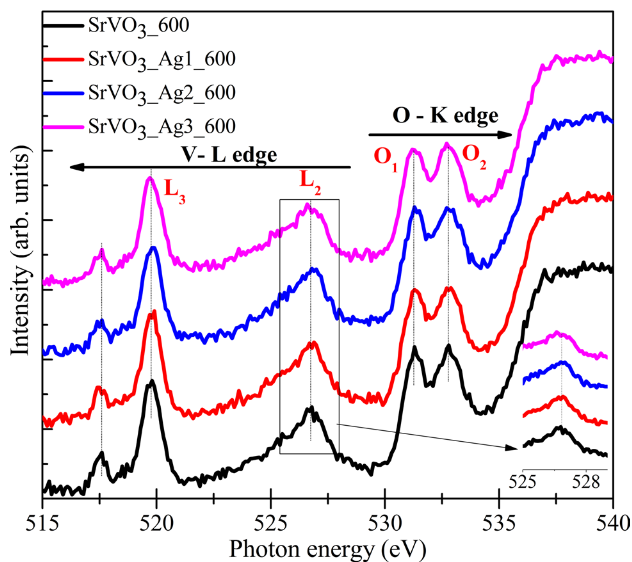

Fig. 3 V L-edge and O K-edge NEXAFS spectra of samples annealed at 600°C: pure $SrVO_3$ ($SrVO_3$_600), 1 × 10^{15} ions/cm^2 implanted $SrVO_3$ films ($SrVO_3$_Ag1_600), 3 × 10^{15} ions/cm^2 implanted $SrVO_3$ films ($SrVO_3$_Ag2_600), and 5 × 10^{15} ions/cm^2 implanted $SrVO_3$ films ($SrVO_3$_Ag3_600). The inset shows a magnified view of the V L-edge.

to the unoccupied V 3*d* levels, respectively. The pre-edge features of the V L-edge (not allowed by selection rules) may appear due to crystal field effects of various V-related defects (i.e., interstitials/stacking faults) in thin films.[4] It is noticeable that the V L_2-edge feature shows broadening/splitting (towards higher energy) upon increasing the Ag^- ion fluence and signifies that Ag implantation has created various defects in the film. The Ag-related defects may have imposed 4*d* states which are overlapping with the V 3*d* levels. There are significant electronic transitions above the V L_2 level which give broadening in the V L_2-edge (see the inset of Fig. 3). Our XRD results have also demonstrated the distortion in the crystallinity of $SrVO_3$ films upon Ag implantation. Therefore, changes in the V L-edge NEXAFS are analogous to the changes in the crystalline properties of $SrVO_3$ films.

The high-energy spectral feature in Fig. 3 (between 528 eV and 540 eV) are due to O K-edge transitions. The O K-edge spectrum originates from O 1*s* transitions to the O 2*p* states which hybridized with the metal *d* states. The O1 peak represents the O 1*s* electronic transitions to the O 2*p* hybridized with metal 3*d* (i.e., t_{2g} orbital; a group of d_{xy}, d_{xz}, and d_{yz} orbitals). Similarly, the O2 peak is due to the O 1*s* electronic transitions to the O 2*p* hybridized with metal 3*d* (i.e., eg orbitals; group of $d_{x^2-y^2}$ and d_{z^2} orbitals).[4,22] It is noticeable that there are no significant changes in the O K-edge spectra of Ag-implanted $SrVO_3$ films. This signifies that Ag atoms are not directly interacting with the O atoms or not making Ag oxides in the $SrVO_3$ films (as supported by XRD studies). This helps us to conclude that Ag implantation in $SrVO_3$ films modifies the electronic structure properties in the higher-energy states to the V 3*d* density of states and that there is no or unnoticeable charge transfer from O atoms to the Ag atoms.

Conclusions

RF sputtering-grown $SrVO_3$ films were implanted with 90 keV Ag^- ions with three different fluences. GIXRD results confirm the Ag implantation induced defect formation in the films and resulted in the diminished XRD peak intensity. The FESEM results convey the rough/pore surface and surface erosion after Ag ion implantation. V L-edge NEXAFS spectra have shown modification in the electronic structure properties of $SrVO_3$ thin films which are reflected as higher-energy broadening/splitting of the V L_2-edge peak. Ag 4*d* levels participated in the V $2p_{1/2}$ electronic transitions to V 3*d* in the Ag-implanted $SrVO_3$ films. The O K-edge spectra are invariant under the Ag implantation-induced modification of the density of states and signify that O atoms are not sharing charges with Ag atoms.

Supplementary Information The online version contains supplementary material available at https://doi.org/10.1007/s11664-022-09454-5.

Acknowledgments Aditya Sharma is thankful to IUAC, New Delhi, India, for providing 90 keV Ag^- ion beam from the low-energy ion beam facility (LIEBF) under the BTR proposal scheme (number 65520). Hyun-Joon Shin would like to acknowledge the support from the National Research Foundation of Korea (NRF- 2015R1A5A1009962).

Conflict of interest The authors declare that they have no conflict of interest.

References

1. K. Yoshimatsu, K. Horiba, H. Kumigashira, T. Yoshida, A. Fujimori, and M. Oshima, *Science* 333, 319 (2011).
2. L. Zhang, Y. Zhou, L. Guo, W. Zhao, A. Barnes, H.T. Zhang, C. Eaton, Y. Zheng, M. Brahlek, H.F. Haneef, N.J. Podraza, M.H.W. Chan, V. Gopalan, K.M. Rabe, and R.E. Herbert, *Nat. Mater.* 15, 204 (2016).
3. M. Wu, J.-C. Zheng, and H.-Q. Wang, *Phys. Rev. B.* 97, 245138 (2018).
4. A. Sharma, M. Varshney, W.C. Lim, H.J. Shin, J.P. Singh, S.O. Won, and K.H. Chae, *Phys. Chem. Chem. Phys.* 19, 6397 (2017).
5. Z.B. Yan, and J.-M. Liu, *Sci. Rep.* 3, 2482 (2013).
6. M. Liu, S.P. Ren, R.Y. Zhang, Z.Y. Xue, C.R. Ma, M.L. Yin, X. Xu, S.Y. Bao, and C.L. Chen, *Sci. Rep.* 5, 10784 (2015).
7. J. Varignon, N.C. Bristowe, E. Bousquet, and P. Ghosez, *Sci. Rep.* 5, 15364 (2015).
8. L. Fagiolari, and F. Bella, *Energy Environ. Sci.* 12, 3437 (2019).

9. U. Lüders, W.C. Sheets, A. David, W. Prellier, and R. Frésard, *Phys. Rev. B* 80, 241102(R) (2009).
10. P. Boullay, A. David, W.C. Sheets, U. Luders, W. Prellier, H. Tan, J. Verbeeck, G. Van Tendeloo, C. Gatel, G. Vincze, and Z. Radi, *Phys. Rev. B.* 83, 125403 (2011).
11. S.Y. Park, A. Kumar, and K.M. Rabe, *Phys. Rev. Lett.* 118, 087602 (2017).
12. D. Srivastava, C. Norman, F. Azough, M.C. Schafer, E. Guilmeau, and R. Freer, *J. Alloys Compd.* 731, 723 (2018).
13. S. Miyasaka, Y. Okimoto, M. Iwama, and Y. Tokura, *Phys. Rev. B* 68, 100406R (2003).
14. C.S. Park, M.H. Hong, H.H. Cho, and H.H. Park, *J. Eur. Ceram. Soc.* 38, 125 (2018).
15. L. Wang, Y. Li, A. Bera, C. Ma, F. Jin, K. Yuan, W. Yin, A. David, W. Chen, W. Wu, W. Prellier, S. Wei, and T. Wu, *Phys. Rev. Appl.* 3, 064015 (2015).
16. D. Ksh, A. Devi, S. Sharma, J. Ojha, A. Parkash, R.K. Vij, and F. Sharma, Singh. *Mat. Lett.* 308, 131283 (2022).
17. A. Sharma, M. Varshney, H.J. Shin, and K.D. Verma, *J. Phys. Chem. Sol.* 75, 1024 (2014).
18. J. Seo, S. Hajra, M. Sahu, and H.J. Kim, *Mat. Lett.* 304, 130674 (2021).
19. S. Chaudhary, H. Saraswat, D. Devi, P. Kulriya, F. Singh, S.O. Won, H.J. Shin, J. Parkash, and A. Sharma, *Vacuum* 179, 109481 (2020).
20. M. Sahu, S. Safranko, S. Hajra, A.M. Padhan, P. Zivkovi, S. Jokic, and H.J. Kim, *Mat. Lett.* 301, 130290 (2021).
21. C. Wang, H. Zhang, K. Deepak, C. Chen, A. Fouchet, J. Duan, D. Hilliard, U. Kentsch, D. Chen, M. Zeng, X. Gao, Y.J. Zeng, M. Helm, W. Prellier, and S. Zhou, *Phys. Rev. Materials* 3, 115001 (2019).
22. H. Saraswat, S. Chaudhary, M. Varshney, D. Devi, F. Singh, S.O. Won, H.J. Shin, and A. Sharma, *Vacuum* 181, 109655 (2020).
23. Y.R. Lu, H.H. Hsu, J.L. Chen, H.W. Chang, C.L. Chen, W.C. Choud, and C.L. Dong, *Phys. Chem. Chem. Phys.* 18, 5203 (2016).
24. A. Sharma, M. Varshney, K.H. Chae, and S.O. Won, *RSC Adv.* 8, 26423 (2018).
25. C. Zou, L. Fan, R. Chen, X. Yan, W. Yan, G. Pan, Z. Wu, and W. Gao, *CrystEngComm* 14, 626 (2012).

Publisher's Note Springer Nature remains neutral with regard to jurisdictional claims in published maps and institutional affiliations.